Structure and Defects in Discotic Crystals and Liquid Crystals As Revealed by Electron Diffraction and High-Resolution Electron Microscopy

I. G. Voigt-Martin,* R. W. Garbella, and M. Schumacher

Institut für Physikalische Chemie der Universität Mainz, Jakob-Welder-Weg 11, D-6500 Mainz, Germany

Received February 6, 1991; Revised Manuscript Received October 15, 1991

ABSTRACT: Both monomeric and polymeric discotic molecules in the crystalline and liquid crystalline phases were investigated by electron diffraction and high-resolution electron microscopy. Analysis of the diffraction patterns indicated the relationship between the orthorhombic, the hexagonal, and the layer-line electron diffraction patterns. The high-resolution images from crystals and liquid crystals showed that the defects which occurred most frequently in the crystals were grain boundaries. These were not observed in liquid crystals. Instead, slight deviations of the molecules from perfect lattice positions disturbed the short-range order while retaining quasi long-range order. Methods are proposed in order to characterize these deviations.

1. Introduction

These investigations were undertaken in order to obtain information about the structure of discotic liquid crystals. Disturbances in lattice statistics lead to the loss of higher order diffraction maxima, and it soon becomes evident that detailed knowledge about the molecular arrangement in the crystalline modification is required before attempting to understand the transition into the liquid-crystalline phase. However, while structural details depend on the precise nature of the particular molecule in question, we hope to show that there are some general features with regard to discotics which should be recognized.

After the first monomeric discotic liquid crystals were described,[1] a large number of polymeric analogues were synthesized. The mesogens were connected with one another either by introducing a flexible spacer in the main chain[2,3] or by connecting them to the polymeric molecule by flexible spacers as side chains.[4] They were initially characterized by DSC measurements and by the textures observed in the light microscope. Subsequent X-ray measurements indicated a hexagonal arrangement of the columns consisting of stacked disks.[5,6] Beside the intercolumn reflections, an amorphous halo indicated a liquidlike arrangement of the aliphatic side chains. The data obtained by electron diffraction for a discotic triphenylene ether gave identical results.[7] These materials can be oriented rather easily in a magnetic field because of their anisotropic diamagnetic polarizability.[8] The molecular motion of the disks in the mesophase can be studied by NMR methods, and it was possible to demonstrate increasing rotation of the triphenylene core about an axis perpendicular to the plane containing the benzene rings as well as increasing motion of the side chains as the temperature is raised.[9,10] It could be shown that the motion of the individual methylene groups increased with an increase in the distance from the core.[11] The free rotation of the core which is observed in monomers is strongly restricted in polymeric analogues by the polymer chain. Possible applications of these materials as photoconductors in a direction along the discotic columns can be envisaged if the stacking of electron-rich triphenylene disks is alternated by electron acceptors such as 2,4,7-trinitrofluorenone (TNF), thus forming charge-transfer complexes.[12-14] Furthermore, if the symmetry of the stacked columns can be broken by tilt in a specific direction and by the addition of a suitable molecule to the triphenylene core, it is possible that second harmonic generation may be induced. For all these purposes, a precise understanding of the molecular structure is essential.

We therefore investigated the two discotic materials depicted in Figure 1 and described in the following:

(1) Sample 1 is a hexakis(heptyloxy)triphenylene monomer.[10,15] This material is crystalline up to 64 °C and then has a narrow mesophase ranging from 64 to 89 °C.

(2) Sample 2 is the polymer corresponding to sample 1. It does not crystallize at all and has a mesophase ranging from 47 to 182 °C. Because of its inability to crystallize (due to inhibitions caused by the polymeric chain), this material can be quenched from the mesophase into the glassy state. For this reason it is possible to obtain high-resolution electron micrographs from the mesophase and not only from the crystalline phase as in case 1.

In order to obtain information about the transition from the crystalline to the discotic phase, sample 1 (monomer) was investigated in the crystalline phase and then heated into the discotic phase. The electron diffraction pattern from this discotic phase was then compared with the discotic phase in the glassy state obtained for the polymer in the diffraction mode.

2. Sample Preparation and Electron Microscopic Technique

In order to avoid dynamical scattering effects, it is essential to prepare very thin films for electron diffraction and imaging. The triphenylene samples were cast on water from dilute solution and subsequently annealed. The films were transferred onto electron microscope grids. The grids were placed in a microoven between the pole pieces of a 2-T magnet and subsequently inserted into the electron microscope. The images were obtained with a Philips 420 STEM in transmission mode. This instrument has a spherical aberration constant of 2 mm. An extremely low electron dose is required for imaging. The critical endpoint dose of these materials is about 6 e/Å^2, so that it is essential to take all the necessary precautions such as cryo methods and low-dose imaging in order to avoid beam damage and, of course, to remain below this dose during imaging.[16] There is a lot of confusion regarding the problem of radiation damage in organic materials:

Radiation damage in polymers during electron-beam exposure is a recognized problem and was first mentioned

0024-9297/92/2225-0961$03.00/0

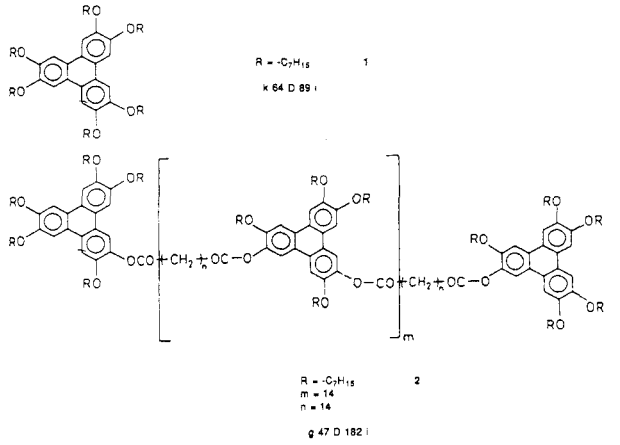

Figure 1. Schematic diagram showing molecular structures of investigated triphenylene derivatives.

in the literature over 20 years ago.[17,18] Detailed measurements of mass and diffraction loss in organic samples by electron energy loss spectroscopy and diffraction have been published by many authors.[19] For this reason, low-dose techniques and cryo methods were developed, which involved (a) the use of a cryoholder for the sample, (b) the employment of a double condensor with a strongly defocused first condensor, and (c) focus of the objective lens in one area of the specimen and photographing an adjacent, previously unexposed area with the first electrons interacting with the sample. It is well-known that extremely low intensities and long exposure times cause the least damage to the sample.

While the above technique is adequate for simple low-resolution work like diffraction and dark-field imaging on unstained samples, they are totally insufficient for high-resolution work, where specimen drift is a problem and a very precise defocus is required.[20]

Moreover, phase-contrast imaging is not achieved in Gaussian focus but in Scherzer focus, which depends very precisely on the frequencies which are to be transferred in the electron microscope. This was achieved by controlling the microscope transfer function with a computer having very fast Fourier transform capabilities attached to the electron microscope via a suitable CCD camera. In our case, the correct transfer function was determined within fractions of a second and the image or diffraction pattern was recorded immediately using a suitable CCD camera or a sensitive emulsion. There have been intense efforts for the past 10 years, especially by biophysicists, to improve these techniques.[21]

This image was used to make an initial estimate of a model for the crystal structure. The molecule is moved and rotated in the proposed unit cell until agreement in diffraction geometry and intensity is obtained with the experimental diffraction pattern.

The coordinates of all the atoms in this improved unit cell (this usually amounts to several hundred atoms) were used as input for the image simulation programs. There has been intense international effort in this field, notably in Arizona,[20] Antwerpen,[22] and Martinsried.[21]

While the dynamical theory of electron diffraction is well established, there are essentially three different computational methods: (1) the eigenstate (Bloch wave) formulation, based on direct solution of the time-dependent Schrödinger equation using Bloch's theorem;[23] (2) the multislice method, based on the physical optics theory of Cowley and Moodie,[24,25] in which the transmission and propagation functions are calculated in successive slices of the crystal in order to obtain the wave field at the exit surface of the crystal; and (3) the real-space physical optics approach of Van Dyck,[22] which starts with the Schrödinger equation and calculates the wave function at successive slices of the crystal.

For the calculations in this work we have used the Van Dyck approach and have shown elsewhere under which conditions the approach is justified for our materials and experimental conditions.[26] In particular, we were able to justify theoretically the use of a highly atypical microscope transfer function, which will be described below.

It was necessary to develop a new method of "high- to medium-"resolution phase-contrast imaging for these materials.[27] The method involves predetermination of the electron microscope phase-transfer function such that a frequency transfer is obtained in the range corresponding to the correct q values by suitable adjustment of the defocus value. (q is the scattering vector $2\pi \sin(\theta/\lambda)$, θ is the scattering angle, and λ is the electron wavelength). A general guide for the best focus setting to image larger objects of dimensions in phase contrast is given by $\Delta f = d^2/2\lambda$. However, in order to interpret the image, it is essential to calculate the full transfer function so that phase reversals and zero image transfer is fully recognized.

Since the q values obtained from organic liquid crystals are in the small-angle range (about 26 Å in real space), it is unfortunately necessary to use phase-contrast functions which behave very badly; namely, Δf can be adjusted to give a frequency window in the correct range, but this maximum is quite narrow and the function oscillates badly at large q values.

It is best to adjust the correct function (which may be different for every sample!) by calculating the Fourier transform of the image on-line, using a suitable video camera attached to a computer with fast Fourier transform facilities.[28]

A direct relationship between the object structure and this high-resolution interference image cannot be assumed a priori. Therefore we compared the images thus obtained with simulated models.[26] Here the interaction of the electron beam with each atom of the proposed unit cell and subsequently the effect of the chosen transfer function on the deformed electron wave at the exist face of the sample were calculated. It was possible to show that, under the imaging conditions used (large defocus, small q values) and for the samples under consideration (small atomic numbers and smeared potential distribution), the image contrast is proportional to the average projected potential distribution in the object, if the thickness d of the object is $\leq 410/Z$ (Å) where Z is the atomic number. In order to build up a model for the simulated images, the unit cell has to be specified. For this, the electron diffraction pattern is required.

Under the specific imaging conditions required for liquid crystals (low-frequency transfer), details in the shape of the molecule will not be observed. However, the positions of the molecules and defects in the crystallographic register (deviations from ideal crystallographic positions, dislocations, and grain boundaries) correspond to the observed images.

The experimental procedure used therefore requires close interaction between these various aspects and is depicted schematically in Figure 2. The sample was placed in a cryoholder, and a low-dose unit ensured that the area to be imaged was not subjected to the electron beam during focusing. On passing through the sample, the electron beam suffers a phase change. For thin organic samples, it is generally appropriate to use the weak phase approximation.[26] Subsequently the diffraction pattern of the

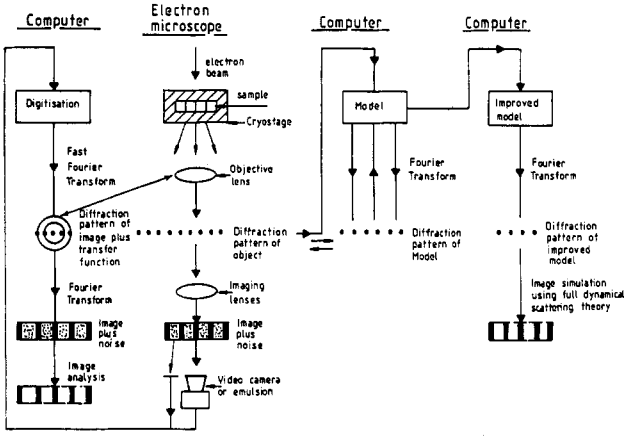

Figure 2. Procedure used for high-resolution electron microscopy, crystallographic determination, and image simulation.

object is formed in the focal plane of the objective lens. This lens produces angle-dependent phase shifts (electron microscope transfer function) which do not affect the diffraction pattern but they do affect the image, which is subsequently produced by the imaging lenses. The image, which always contains noise, was recorded on a sensitive emulsion or by a video camera. The computer indicated on the left of the electron microscope repeated this process with the image. First, a Fourier transform of the image produced its diffraction pattern plus the microscope transfer function. This appears on a screen, and the microscope parameters are corrected until an appropriate transfer function is found. This requires a computer capable of performing extremely fast Fourier transform, because the correct defocus value must be found before the specimen is destroyed. A second Fourier transform then produces the image, including noise. Image analysis in real or reciprocal space (or a combination of both) can be used to eliminate the noise. Many different procedures have been described to cope with the problem.[29-31]

The diffraction pattern of the object was now used to propose an initial structure. The molecule is first built up with a suitable molecular modeling program. In this case INSIGHT and DISCOVER were used and several minimization processes initiated before selecting the final molecular structure. This molecule was then placed in a unit cell which seemed appropriate from the experimental diffraction pattern. Generally a low symmetry is used initially. The molecules were then rotated and shifted using CERIUS, a program enabling direct observation of the changing diffraction pattern as the unit cell is adjusted. For this program good graphic display and high speed are essential. It was originally developed for X-ray diffraction and has now been extended to incorporate electron diffraction. We are currently performing a comparative study of results obtained using CERIUS with those from MULTISLICE calculations and the Van Dyck procedure. When agreement between the calculated and experimental diffraction pattern was reached, the cell symmetry and space group were determined. The coordinates of all the atoms in real space obtained from this procedure were now used as input for the simulation procedures. We have used the physical optics approach developed by Van Dyck[22] in order to calculate the full dynamical diffraction pattern and image as a function of the sample thickness and defocus value obtained from the first computer. At this stage the microscope transfer function is accounted for and the calculated image should agree with the experimental image except for the noise.

3. Results

3.1. Electron Diffraction from Monomer in the Crystalline and Discotic Phase. We have already pointed out in previous papers[7,26] that there is a dramatic loss of higher order diffraction maxima when these substances pass from the crystalline into the liquid crystalline phase, while, however, the peak sharpness is retained. Therefore, in order to learn something about the microscopic structure of the liquid crystalline phase, it is necessary to understand why the higher order maxima are so strongly damped with simultaneous retention of an extremely narrow peak width. In a general way it is clear that this phenomenon must be related to a loss of symmetry and translational correlations. However, detailed understanding can only be achieved if the structure of the crystal is well-known.

In the case of monomeric oriented systems with disk-shaped mesogenic groups, the material can crystallize and the molecules form cylindrical columns.

The situation is quite complex for triphenylenes with an ether group in the side chain ($R = -C_7H_{15}$). This sample gives rise to two different diffraction patterns. Sometimes a unit cell with orthogonal axes (Figure 3a) is observed. There are many higher orders; the two intense inner reflections correspond to distances of 38.3 and 32.6 Å.

Frequently another diffraction pattern is observed in adjacent regions of the same sample (Figure 4) in which a number of diffraction spots on the equator and two layer lines are observed. The two innermost maxima on the equator correspond to a d spacing of 16.3 Å.

This diffraction pattern changes completely when the sample is heated into the discotic phase (Figure 3b), where the familiar hexagonal pattern is obtained with only first- and second-order sharp maxima. Close inspection of the intensities reveals that they are not all identical, so that while the geometry is hexagonal, the symmetry is not.

3.2. High-Resolution Images of Monomer in the Crystalline Phase. We have discussed previously the enormous difficulties encountered when trying to obtain images from these beam-sensitive samples and how these can be overcome.[27]

Figure 5 shows an image of the triphenylene ether derivative. The high-resolution micrograph indicates distinct grains: (1) A region giving rise to the orthogonal diffraction pattern with two sets of perpendicular perfectly straight lines. There is a grain boundary surrounding this region. (2) In addition to this there are two sets of straight lines at an angle of 60° and another set of straight lines at 30° to the previous ones in the other grains above and below the central one. The grain boundary, indicated in the copy of the transparent overlay, contains many defects. More frequently (Figure 6) regions are observed where only one set of lines is observed in each of the three different grains related by 60° to its neighbor. The inset shows the microscopic diffraction pattern from the regions indicated. The nature of the grain boundary is indicated in the copy of the transparent overlay.

Clearly it is impossible to obtain high-resolution images from the monomeric samples in the liquid discotic phase.

3.3. Electron Diffraction and High-Resolution Images from Discotic Triphenylene Polymer in the Glassy State. While the discotic monomer crystallizes when it solidifies, the polymeric material with an identical triphenylene molecule can be retained in the discotic phase when solidified, thus enabling high-resolution imaging to be performed. The diffraction pattern is identical in character to the one obtained from the monomer in the liquidlike discotic phase (Figure 7, inset). Since the dis-

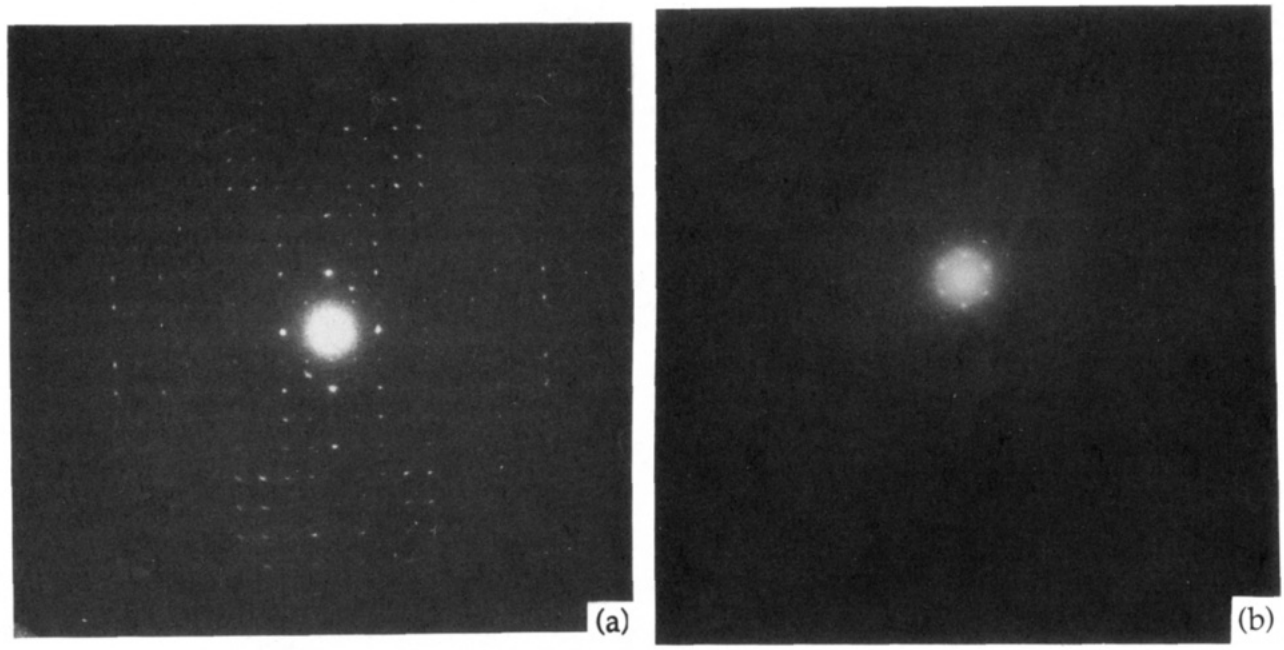

Figure 3. Diffraction pattern obtained from a hexakis(heptyloxy)triphenylene monomer (sample 1) (a) in the crystalline phase and (b) in the liquid crystalline phase.

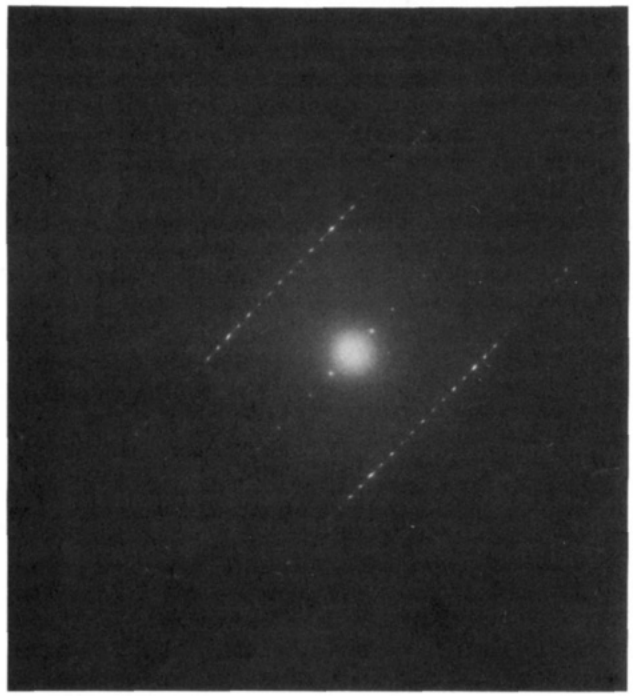

Figure 4. Diffraction pattern obtained from a hexakis(heptyloxy)triphenylene monomer (sample 1) in the crystalline phase showing a different zone.

cotic polymer was quenched into the glassy state, it is possible to obtain high-resolution images. This is shown in Figure 7. It is clear that the arrangement of the columns appears at first glance to be hexagonal. An oblique glance down the columns indicates deviations from the absolutely straight planes which were observed in the crystals.

4. Discussion

4.1. Crystal Structure. Determination of a crystal structure giving rise to the observed diffraction patterns and involving 90 atoms/molecule made the use of sophisticated computer facilities mandatory. The CERIUS programs used for these calculations were obtained from Cambridge Molecular Design and enabled real-time diffraction simulations to be performed such that the molecule in the proposed model structure could be tilted and shifted while observing the changes in diffraction intensities on-line. In view of the large number of atoms per molecule, only three carbon atoms were retained in each of the side chains.

It was possible to simulate the two diffraction patterns identical to those obtained experimentally from our samples in the crystalline phase: the orthogonal pattern of Figure 3a and the layer-line pattern of Figure 4. Clearly, these represent different zone axes of the same crystal structure. Only one model structure viewed from the (001) (disks parallel to film plane) and (100) (disks perpendicular to film plane) zones could reproduce identical intensities and symmetries. These two projections are shown in Figures 8 and 9.

In order to reproduce the strong intensities on the first layer line, a tilt of the triphenylene molecule in both directions has to be invoked. The angle is ±47°. For this reason the c-axis distance is increased from 3.4 Å (distance between triphenylene cores) to 5 Å (Figure 8 showing the (001) zone). At the same time the experimental diffraction pattern indicates missing h = odd reflections in the orthogonal diffraction pattern so that the cell is face-centered on one face and can be simulated by the above model in the (100) zone.

The calculated cell parameters and symmetry, which are closest to the observed diffraction patterns, can be summarized as follows: cell symmetry, $Ama2$; International Tables No. 40; lattice type, orthorhombic; point group, $mm2$; lattice centering, A centered; lattice points, $(0, 0, z)$, $(^1/_2, 0, z)$; symmetry positions, (x, y, z), $(x + ^1/_2, -y, z)$; number of molecules per cell, 4. The lattice parameters are a = 38.3 Å, b = 32.6 Å, c = 5 Å, and $\alpha = \beta = \gamma = 90°$.

For this proposed cell containing four triphenylene molecules which are tilted at an angle of ±47° to the ab plane while the stacked columns remain perpendicular to this plane, the agreement between theory and experiment is quite good. Some details in the outer regions of the diffraction pattern are not quite satisfactory. Therefore

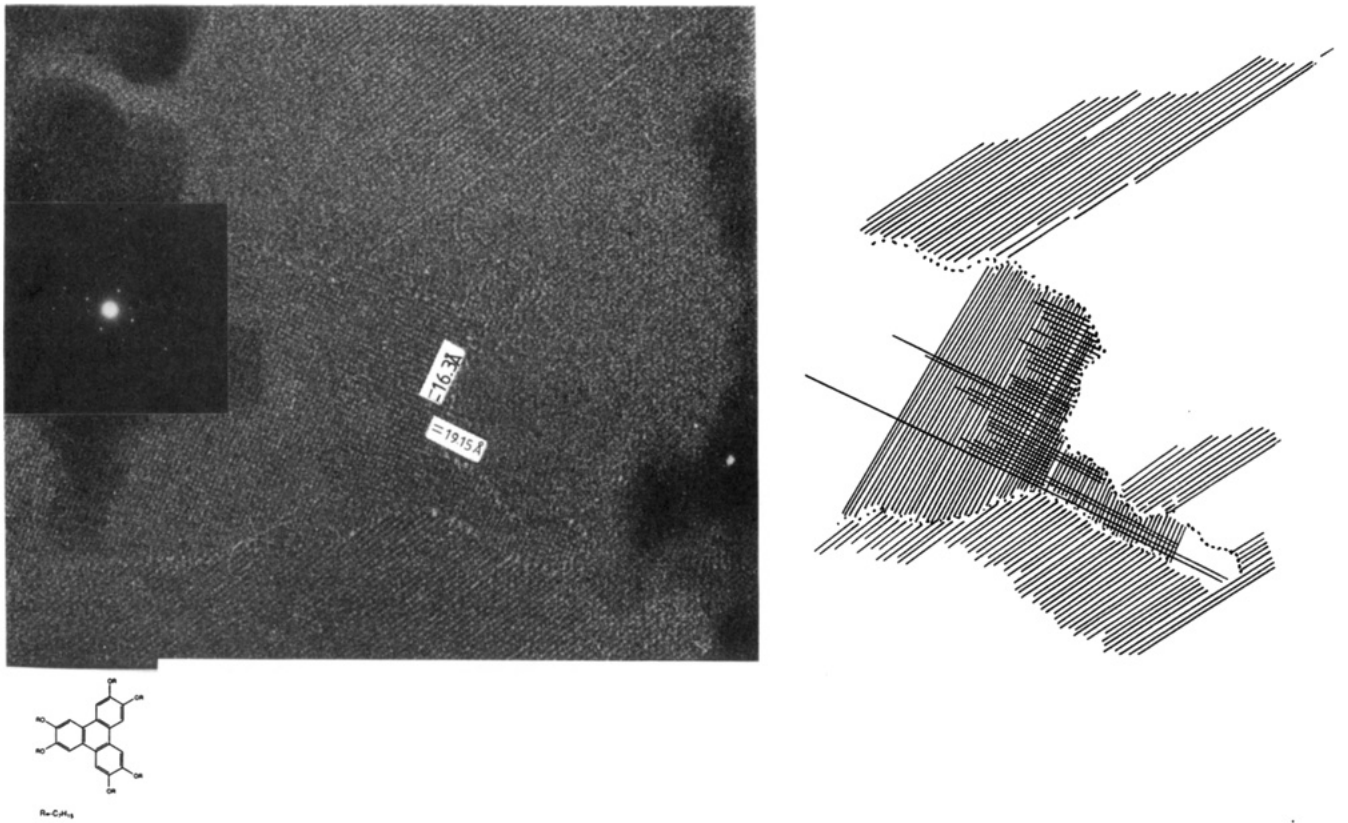

Figure 5. High-resolution image obtained from a hexakis(heptyloxy)triphenylene monomer (sample 1) crystal with its electron diffraction pattern (inset).

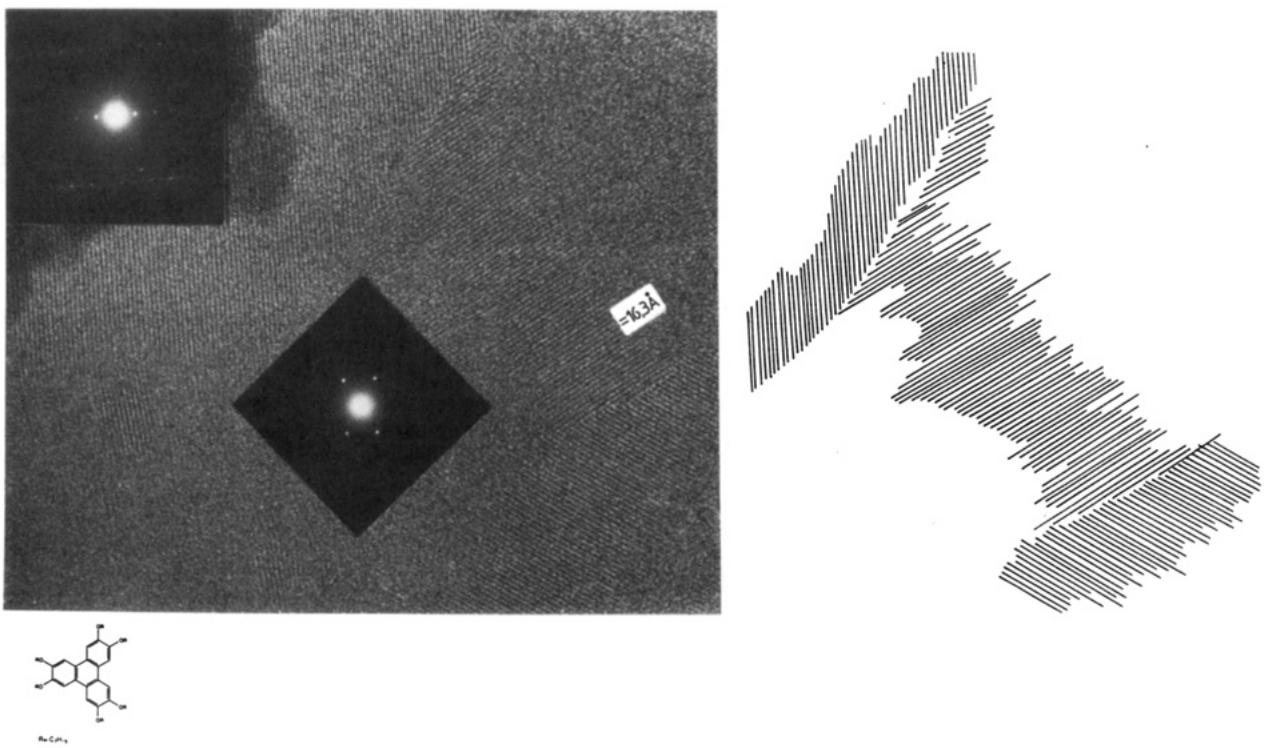

Figure 6. High-resolution image obtained from a hexakis(heptyloxy)triphenylene monomer (sample 1) crystal with its electron diffraction pattern (inset).

a diffraction pattern from the same model, taking account of dynamical scattering, was calculated (Figure 10). The agreement between calculated and experimental diffraction patterns was then improved.

It is important to note that the most frequent observation of the (100) zone indicates that the discotic disks generally lie perpendicular to the film plane (i.e., columns *in* the film plane).

On raising the temperature, the sample is brought into the discotic phase. The experimental diffraction pattern changes drastically: (1) All higher order reflections are lost. (2) The remaining diffraction spots remain sharp. (3) The symmetry changes from orthorhombic to "pseudo-hexagonal" (Figure 3b).

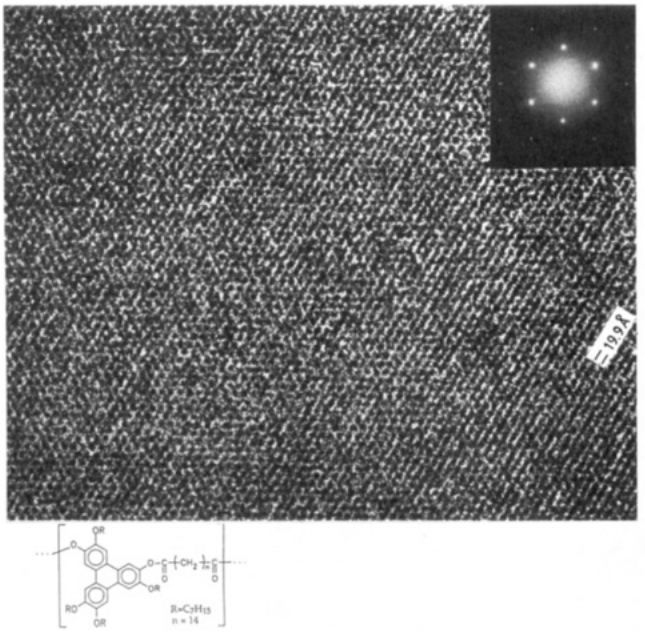

Figure 7. High-resolution image obtained from a hexakis(heptyloxy)triphenylene polymer (sample 2) liquid crystalline glass with its electron diffraction pattern (inset).

In order to explain the change from a face-centered orthorhombic to a hexagonal cell, it was necessary to invoke a shift of $a/4$ along the a axis and an expansion of the lattice constant to $a = 39.2$ Å and $b = 22.6$ Å. This causes the change in the diffraction pattern indicated in Figure 11. In order to obtain hexagonal symmetry, it is necessary only to propose a loss of orientational correlations of the individual molecules, leading immediately to a lower symmetry, or to allow the molecules to lie flat (Figure 11). This can be expected to happen when the molecules pass into the liquid phase and rotate about an axis perpendicular to the triphenylene core.

Finally, the diffraction pattern obtained from the polymeric liquid crystal in the glassy state is *identical* to that obtained from the monomeric material in the high-temperature liquid crystalline phase. Only the cell constants are larger, with $a = 39.8$ Å and $b = 23.0$ Å.

The enlargement of the cell constant is to be expected because the polymer chain has to be incorporated between the columns of stacked disks. We can, therefore, propose with some justification that the cell is similar to the one proposed for the high-temperature monomeric discotic phase and that the polymers are not capable of performing the massive reorientations and translations required to pass from the hexagonal arrangement in the liquid phase with disks parallel to the film plane into the orthogonal phase with disks perpendicular to the film plane. This arises because of kinetic restrictions imposed by the polymer chain. It was not possible to establish with certainty whether disordered disks in the discotic phase are still tilted with respect to the columns, but certainly a very good fit with experimental data can be obtained if the disks are assumed to lie flat.

4.2. Simulation of Images. In a previous paper we have discussed the problems involving interpretation of high-resolution images, particularly when large defocus values are used which are needed in order to image details in the small-angle range of reciprocal space.[26] The image is a very complex interference pattern, and it cannot be assumed a priori that it represents a projection of the potential distribution in the sample. For this reason, it is essential to perform image simulation taking account of *dynamical scattering* effects and of *all instrumental parameters* effecting the image. In order to do this, a theoretical approach developed by Van Dyck was used.[22,32,33]

The coordinates of all the atoms in the unit cell as determined in the previous section were used as input for the Van Dyck simulation programs, taking full account of dynamical scattering. The microscope transfer function was calculated and all optical parameters included to calculate the images for various sample thicknesses and defocus values.

The diffraction patterns and images of the crystallographic zones determined in the previous section were calculated. The results are shown in Figures 10 and 12. They indicate excellent agreement between theory and experiment. The diffraction patterns show the orthorhombic and layer-line patterns in the (001) and (100) zones, respectively (Figure 10), giving rise to the cross-hatch and line patterns (Figure 12) observed experimentally in Figures 5 and 6 at the defocus values which were used experimentally. The detail in the calculated images is better than that in practice because the optical parameters chosen were better than those which we can achieved in practice.

4.3. Characterization of Defects Observed in High-Resolution Images of Discotic Systems. The most obvious defects in the crystalline phases of discotic systems are grain boundaries (Figures 5 and 6).

The defects in the liquid crystalline phase (Figure 7) are more difficult to perceive and quantify. Grain boundaries were never observed in the liquid crystals. However, it is clear from the high-resolution electron micrographs that the perfect registry typical of the crystal is disturbed by very small deviations of the discotic columns from the ideal lattice positions. The difficulty now arises as to how deviations can be characterized. We have approached this problem by using two correlation techniques, which will be described in the following:

(a) Autocorrelation Function. The autocorrelation function (ACF) of a function (r) is given by

$$\rho(r) = \int f^*(r_1)\, f(r_1+r)\, \mathrm{d}r_1 \qquad (1)$$

which is a measure of the correlation between the values of a function at values of a variable differing by an amount r.

In the case of a periodic image, the ACF shows a peak repeated on the periodic lattice and its location relative to the origin marks the translation vector for complete overlap.

The intermediate state is one in which there are no correlations beyond a distance L. In that case, $\rho(r)$ tends toward zero since the product $f(r_1)\, f(r_1+L)\, \mathrm{d}r_1$ must be zero. The shape of the correlation function therefore summarizes statistical information about a characteristic correlation length L. This is shown schematically in Figure 13.

In the case of an electron micrograph, the image is digitized by recording the image density $\rho(r)$ obtained from the emulsion gray levels (which are proportional to the electron dose in the linear region of the emulsion) in an array consisting of at least 512 × 512 digital points.

The integral of (1) is evaluated and repeated for all displacement vectors, resulting in a two-dimensional function (essentially the Patterson function), which can be displayed using gray tones. In any specific direction these gray tones are converted into intensities as a function of distance x (1D ACF) and therefore give a rather clear indication of the correlation length L.

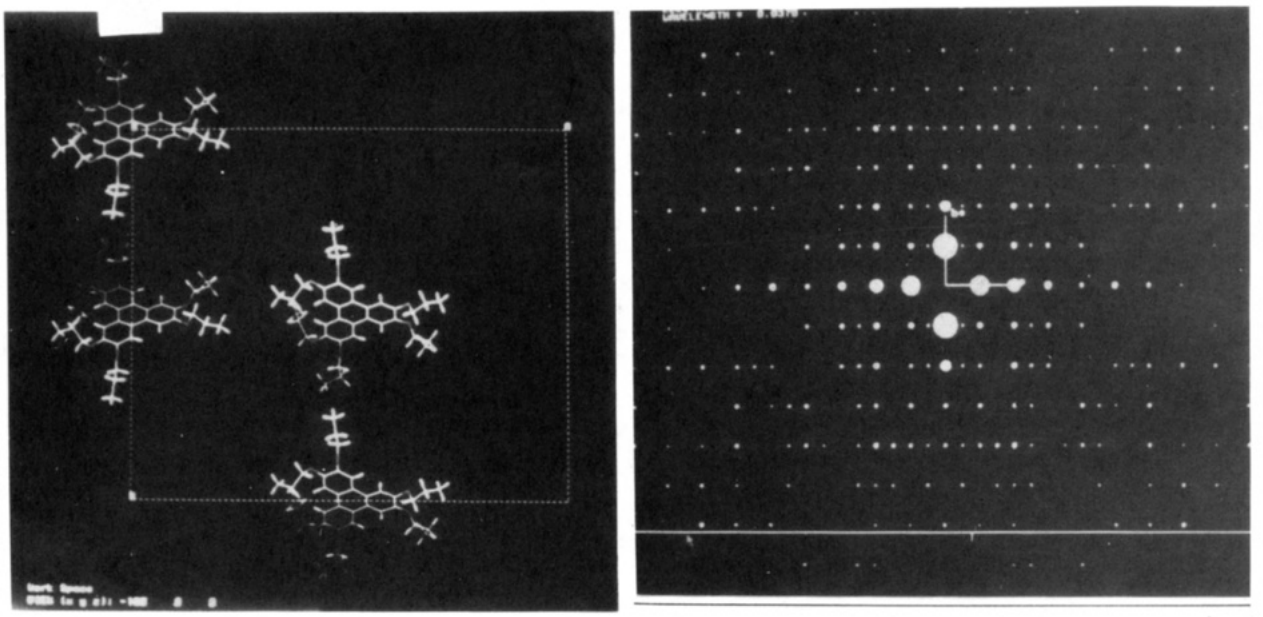

Figure 8. Simulated diffraction patterns from a triphenylene monomer arranged as shown in the schematic giving an orthogonal diffraction pattern [(001 zone].

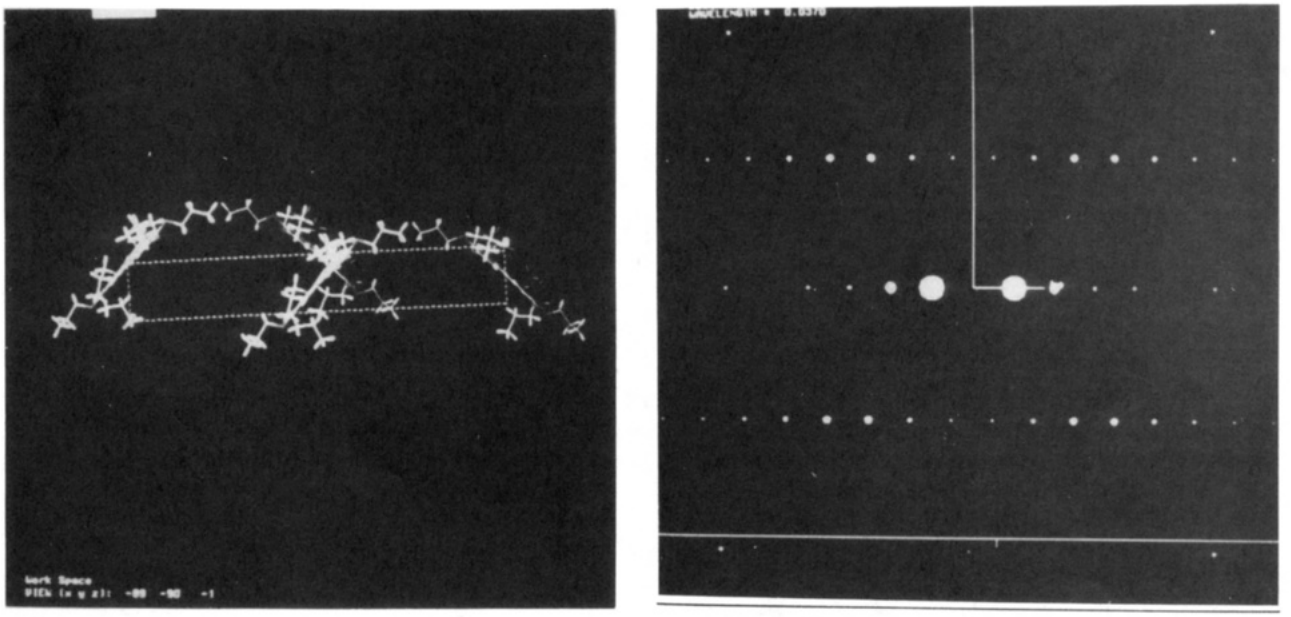

Figure 9. Simulated diffraction pattern from a triphenylene monomer arranged as shown in the schematic giving a layer-line pattern [(100) zone].

By using this technique on the images from a perfect crystal (Figure 5) and the liquid crystal (Figure 7) the 2D and 1D autocorrelations in Figure 14 were obtained. It is clear that the liquid crystal seems to be characterized by a slow decrease in correlations beyond a distance of several hundred ångstroms.

(b) Deviation Vectors. Another technique which we consider useful in order to characterize the lattice distortions in liquid crystals is one using deviation vectors,[34] a method which K. Downing at Berkely has used to perform some preliminary work on our liquid crystal image of Figure 7. Selected areas were densitometered on a flat-bed microdensitometer. The optical density measurements were truncated and packed into a dense format. The Fourier transform of the image is calculated and displayed. Frequency filtering is applied by using a suitable mask around all strong reflections. All other parts of the transform are set to zero, including the $F(0,0)$ term. The filtered image is calculated by back-transformation and the central area boxed off to provide the reference area. This was then correlated with equivalent areas of the whole image, and a cross-correlation map was obtained.[34] Finally, vector displacements of the centers of gravity of correlation peaks from positions predicted based on a perfect lattice are plotted (Figure 15). The deviations are extremely small fractions of the lattice constants and are therefore magnified in these maps in order to make them visible. The light areas are regions which are in good register with the reference area (in the center of the picture). The dark areas indicate shift with respect to the reference area. It is important to note that in some areas there is clear evidence of *lateral shift* (parallel displacement vectors) whereas other areas indicate a slow variation in the direction of the vector (i.e., *rotation* with respect to the reference area).

Therefore, the deviation vectors supply even more information than only that concerning the size of the correlated regions: They give precise information about

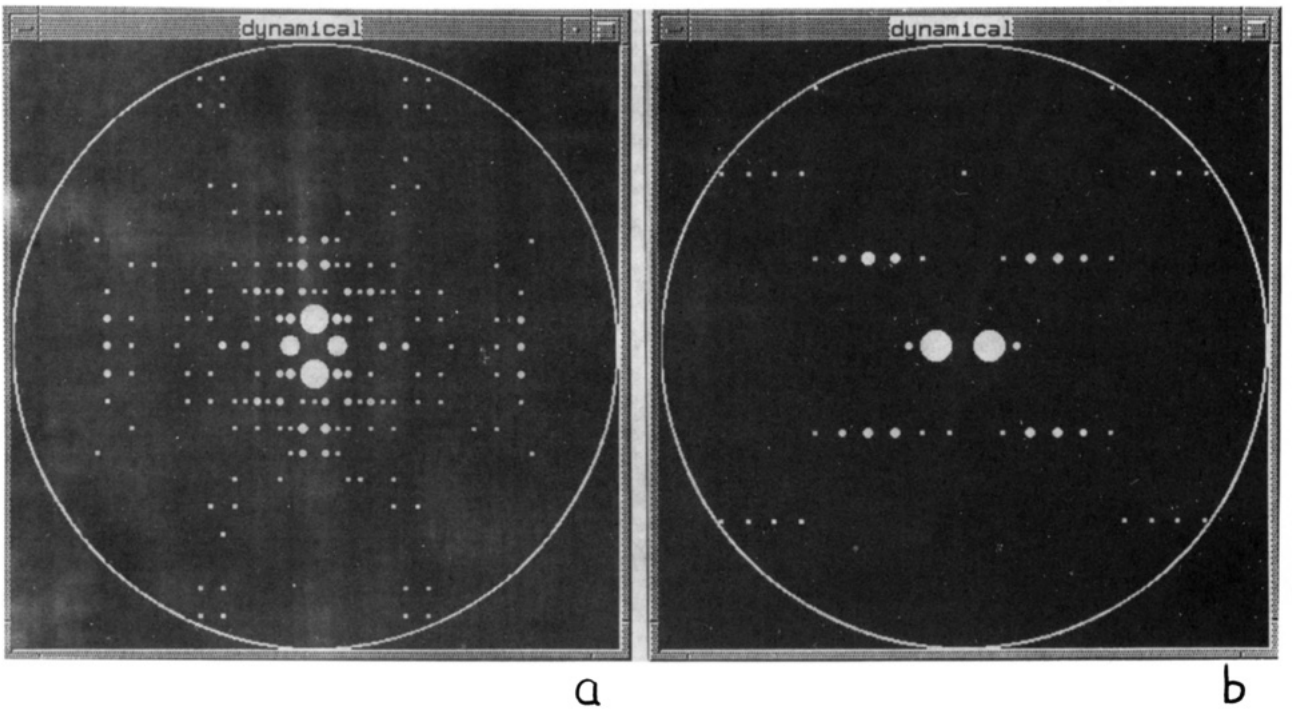

Figure 10. Simulated diffraction pattern from a triphenylene monomer arranged as shown in Figures 8 and 9, taking account of dynamical scattering: (a) (001) zone; (b) (100) zone.

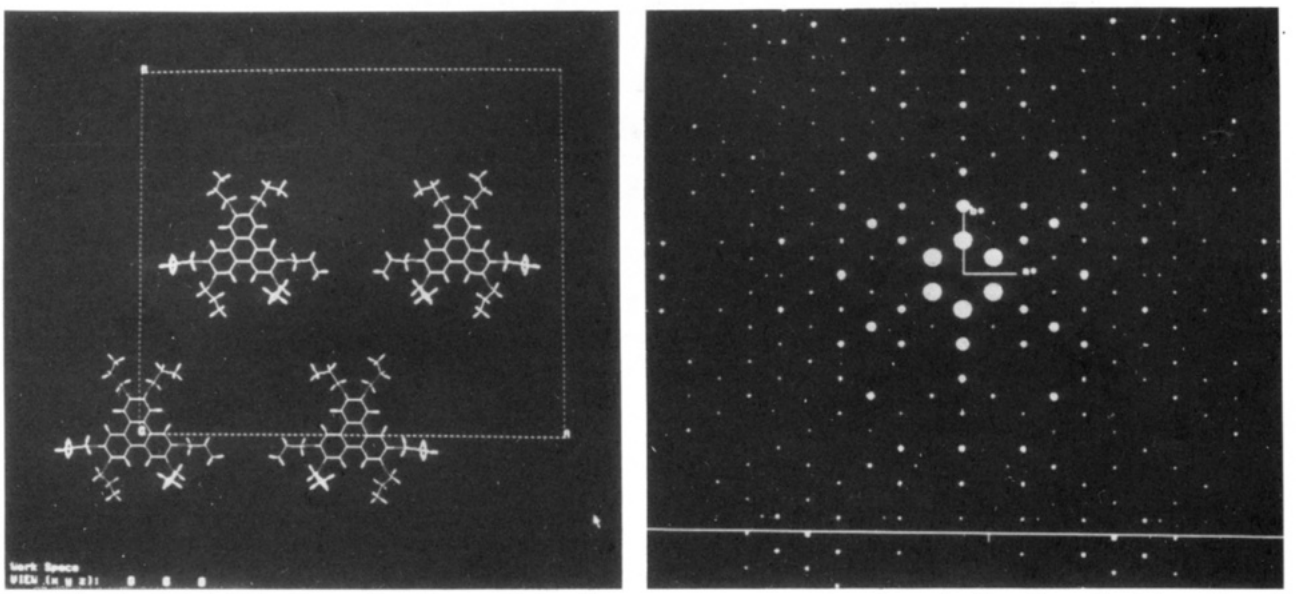

Figure 11. Simulated diffraction pattern from a triphenylene monomer arranged as shown in the schematic giving a "pseudo-hexagonal" diffraction pattern.

details of the deviations from ideal lattice sites. In order to determine to what extent the deviations are related to the original thermal motion of the molecules in the discotic phase or to the transition into the glassy state, a detailed study of these vectors as a function of the cooling procedure will be required.

5. Conclusions

In this work, both selected area electron diffraction and "high"-resolution imaging have been used to obtain a maximum amount of information about the structure of crystalline and liquid crystalline discotic systems and to obtain some information about the lattice statistics. In a previous paper[35] we have discussed at some length the intensity distribution and contour shape to be expected in the electron diffraction pattern for three different lattice statistics with specific lattice defects: (I) the polycrystalline phase; (II) the Nelson and Halperin (NH) theory of hexatic smectic mesophases; and (III) the paracrystalline concept of Hoseman and Bagchi. In the LB monolayers with a hexagonal symmetry which were considered there, the best agreement between theory and experiment was achieved for the NH model of an interacting gas of dislocations. For the present case of the hexagonal discotic mesophase none of the above models applies: The high-resolution micrographs do not indicate a high density of dislocations, and the diffraction spots are extremely sharp. The only feature typical of both cases is a loss of higher order maxima. It appears more appropriate in this case to apply lattice statistics derived by Selinger and Bruinsma[36] in which a continuum theory is used to calculate static correlation functions in the hexagonal dis-

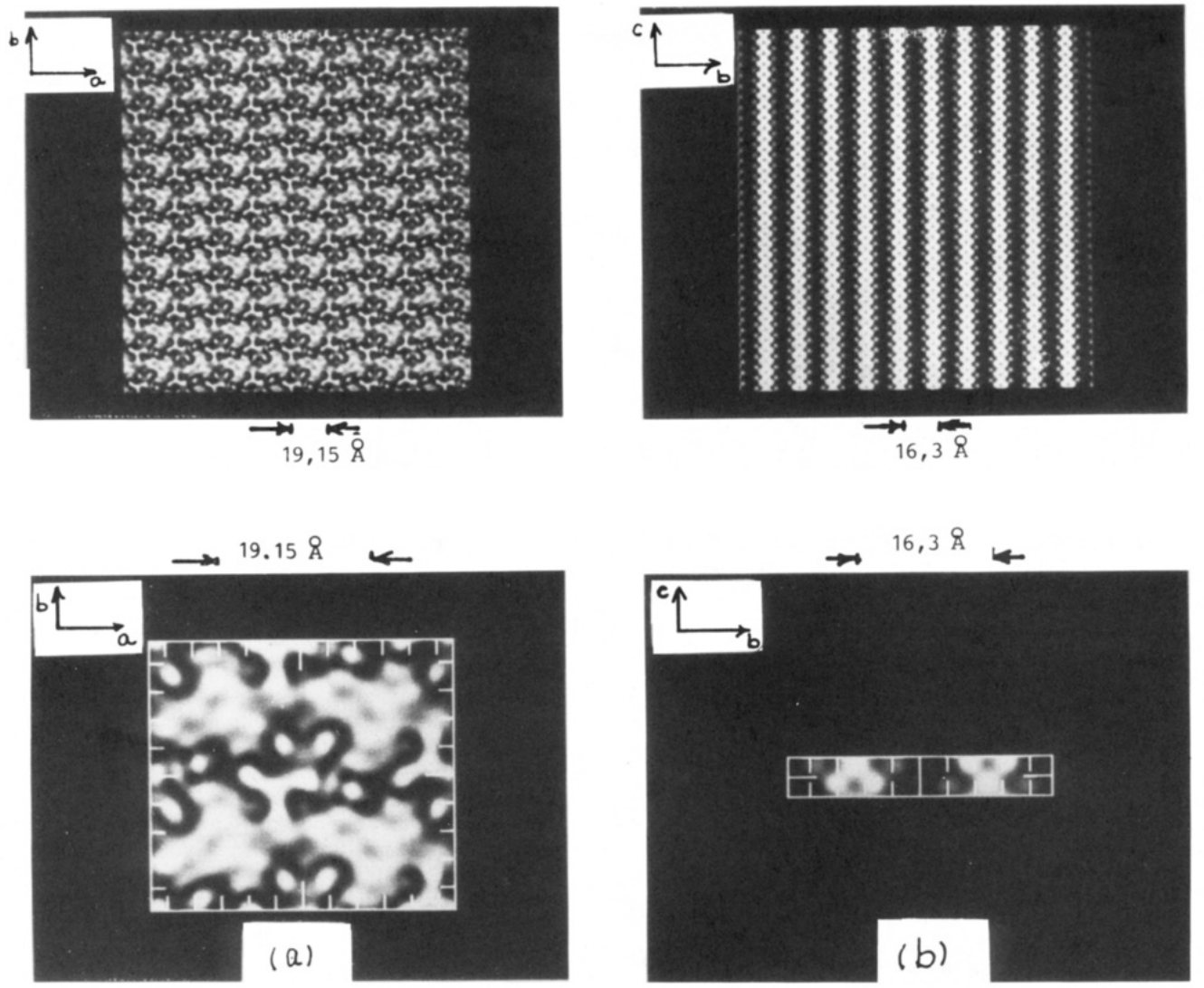

Figure 12. Simulated images from a (001) zone (a) and a (100) zone (b).

cotic liquid crystal phase. After appropriate Fourier transformation, the structure factor near a nonzero 2D reciprocal lattice vector **G** is given by

$$(\mathbf{G}+\mathbf{k}_\perp,k_z) \approx \rho_0^2 e^{-G^2(|u|^2)/2} \times \left[(2\pi)^3\delta^{(3)}(\mathbf{k}) + \frac{k_B T B_\alpha G_\beta P^L_{\alpha\beta}(\mathbf{k}_\perp)}{(\lambda+2\mu)k_\perp^2 + K_1 k_\perp^2 k_z^2 + K_3 k_z^4} + \frac{k_B T G_\alpha G_\beta P^T_{\alpha\beta}(\mathbf{k}_1)}{\mu k_\perp^2 + K_2 k_\perp^2 k_z^2 + K_3 k_z^4}\right]$$

where $q_\perp$ and q_z are the tangential and radial reciprocal lattice vectors with $\mathbf{q} = \mathbf{G} + K$, λ and μ are the Lamé constants, and $k_\perp$ and k_z are the elastic constants.

$$P^L_{\alpha\beta}(q_\perp) = \frac{q_\alpha q_\beta}{q_\perp^2}, \quad P^T_{\alpha\beta}(q_\perp) = \delta_{\alpha\beta} - \frac{q_\alpha q_\beta}{q_\perp^2}, \quad \alpha,\beta = x,y$$

Therefore the intensity profile consists of a δ diffraction peak at each reciprocal lattice vector, surrounded by diffuse thermal scattering. The reduced stability of the system is due to undulations of the columns, which enhance the diffuse thermal scattering. The deviations of the centers of mass from true lattice positions in a projection viewed from above as observed in our experiments may reflect this lack of correlation down the column and leads to a loss of higher order maxima. Why then did we not analyze the diffraction profiles as in our previous work rather than simply noting that the diffraction spots are extremely sharp? The reason is that an analysis involving an "infinitely" intense diffraction spot with all the physical information contained in the wings is virtually impossible using electron diffraction. The large intensity in the peak leads to a spread in the photographic emulsion which depends on details of the emulsion and exposure time. The "electron diffusion" thus produces a probability distribution extending over several grains and which must be calculated for each situation.[37] This spread would, of course, affect the intensity in the wings. In addition to this, the small effect of the diffuse scattering in the wings is very difficult to detect above the general noise in the emulsion. It therefore made much more sense to study the images directly and attempt to analyze the deviation

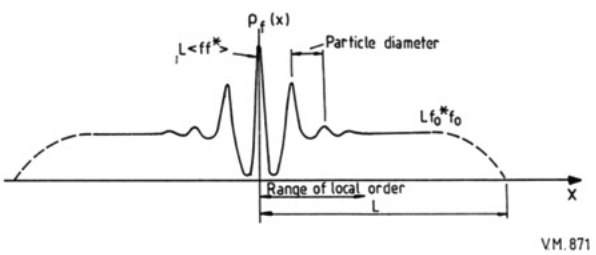

Figure 13. Schematic diagram showing correlation $\rho(r)$ between the values of a function $f(r_1)$ at values of a variable differing by an amount r (Champeney, D. C. *Fourier Transforms and Their Physical Applications*; Academic Press: New York, 1973).

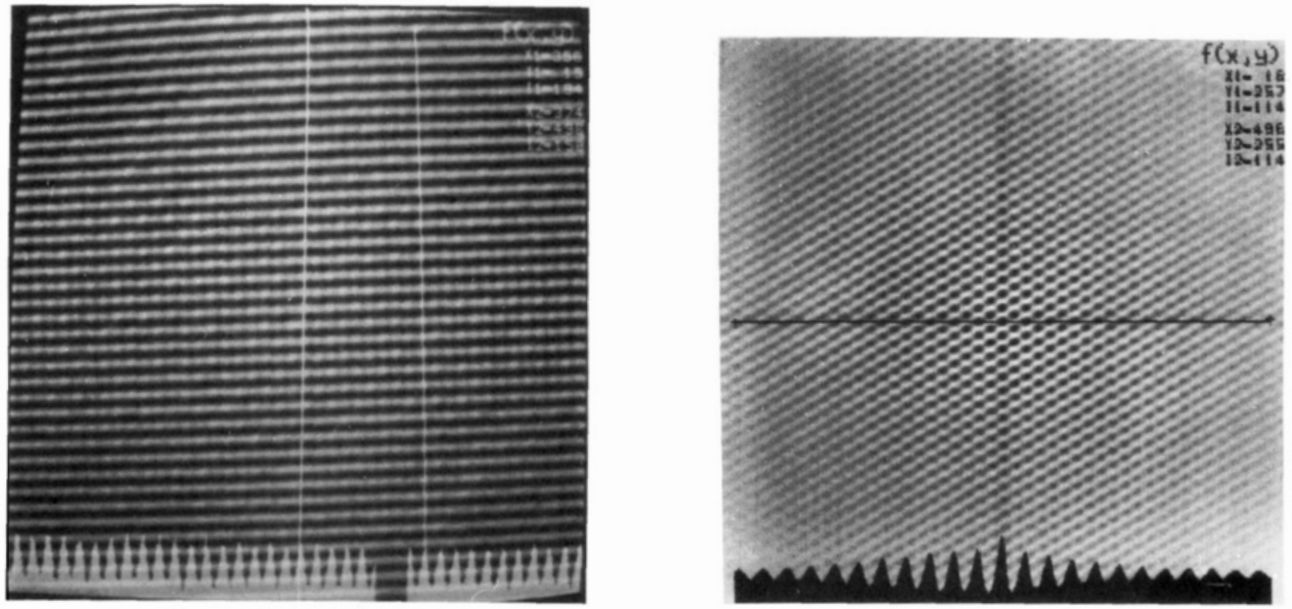

Figure 14. Autocorrelation functions obtained from images of a perfect crystal (Figure 5) and liquid crystal (Figure 7).

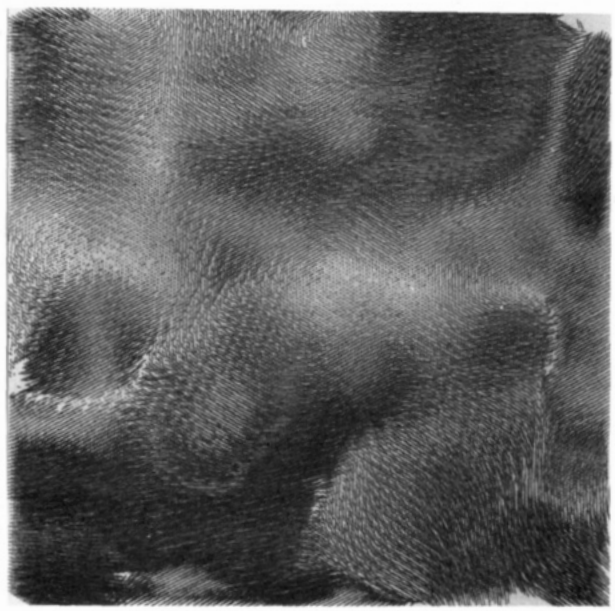

Figure 15. Calculated deviation vectors obtained from the image of a liquid crystal in Figure 7.[34]

vectors. However, it is possible to analyze less intense electron diffraction profiles and even obtain pair distribution functions from them, as we have shown previously.[38]

Because these samples are very beam-sensitive, special precautions involving cryo and low-dose imaging were applied and new experimental procedures adopted. The conclusions can be summarized as follows:

(1) Electron diffraction patterns from two zone axes in the crystalline phase and one "zone axis" in the discotic phase were obtained.

Structure analysis of crystalline samples indicated a face-centered *Ama*2 orthothrombic unit cell with lattice parameters a = 38.3 Å, b = 32.6 Å, and c = 5 Å. The layer-line patterns indicate that the triphenylene core within the columns are tilted at an angle of 47° with respect to the ab plane but the columns are perpendicular to this plane.

(2) Generally the triphenylene molecules in the crystalline phase lie perpendicular to the film plane (i.e., columns in the film plane). The monomers in the discotic phase all show sharp reflections with "hexagonal symmetry" in which the triphenylene molecules lie in the film plane (i.e., columns perpendicular to the film plane). The change involves both translation and rotation of the individual molecules.

(3) The polymer quenched from the liquid crystalline phase has the same diffraction pattern as the monomer in the liquid crystalline phase.

(4) The loss of higher order diffraction maxima in the discotic phase as viewed perpendicular to the columns indicates that the projected columns do not occupy perfect "lattice" sites. The retention of peak sharpness indicates that translational correlations perpendicular to the columns are quite long range. However, there may well be an absence of correlations along the axes of the columns which were not observed in these experiments.

(5) Correlation analysis of the images also indicates quasi-long-range order.

(6) The high-resolution images calculated from the proposed model structures agree well with the experimental images.

(7) Images from crystals show perfect order (either cross-hatch images in the (001) zone or straight lines in the (100) zone within crystallographic grains.

(8) Typical defects in crystals were shown to be grain boundaries.

(9) Images showing details of the structure of the grain boundaries in crystals were obtained.

(10) Grain boundaries were never observed in liquid crystalline discotic systems.

(11) The projected centers of gravity of the columns in the glassy discotic polymer systems situated on a quasi-hexagonal lattice were slightly displaced from perfect lattice sites, and the deviations indicated a very small lateral shift of only a fraction of a lattice spacing as well as a slow rotation of the deviation vector.

Acknowledgment. We are very much indebted to Prof. H. W. Spiess for kindly giving us these samples. The use of the IRIS work station at the DKI Darmstadt (Prof. J. H. Wendorff) and the help of Dr. K. Downing at Berkley in obtaining the deviation vectors are gratefully acknowl-

edged. The simulations were performed with the programs developed at Antwerp University (Prof. D. Van Dyck). Financial support (M.S. and R.W.G.) by the Deutsche Forschungsgemeinschaft within the framework of SFB 262 is gratefully acknowledged.

References and Notes

(1) Chandrasekhar, S.; Sadashiva, B. K.; Suresh, K. A. *Pramana* **1977**, *9*, 471.
(2) Kreuder, W.; Ringsdorf, H.; Tschirner, P. *Makromol. Chem., Rapid Commun.* **1985**, *6*, 367.
(3) Wenz, G. *Makromol. Chem., Rapid Commun.* **1985**, *6*, 577.
(4) Kreuder, W.; Ringsdorf, H. *Makromol. Chem., Rapid Commun.* **1983**, *4*, 807.
(5) Herrmann-Schönherr, O.; Wendorff, J. H.; Kreuder, W.; Ringsdorf, H. *Makromol. Chem., Rapid Commun.* **1986**, *7*, 97.
(6) Hüser, B.; Pakula, T.; Spiess, H. W. *Macromolecules* **1989**, *22*, 1960.
(7) Voigt-Martin, I. G.; Durst, H.; Brzezinski, V.; Krug, H.; Kreuder, W.; Ringsdorf, H. *Angew. Chem.* **1989**, *101*, 332.
(8) Hüser, B.; Spiess, H. W. *Makromol. Chem., Rapid Commun.* **1988**, *9*, 337.
(9) Kranig, W.; Boeffel, C.; Spiess, H. W. *Macromolecules* **1990**, *23*, 4061.
(10) Kranig, W.; Hüser, B.; Spiess, H. W. *Adv. Mater.* **1990**, *2*, 36.
(11) Hsu, T.-C.; Hüser, B.; Pakula, T.; Spiess, H. W.; Stamm, M. *Makromol. Chem.* **1990**, *191*, 1597.
(12) Ringsdorf, H.; Wüstefeld, R.; Zerta, E.; Ebert, M.; Wendorff, J. H. *Angew. Chem.* **1989**, *101*, 934.
(13) Bengs, H.; Ebert, M.; Karthaus, O.; Kohne, B.; Praefcke, K.; Ringsdorf, H.; Wendorff, J. H.; Wüstefeld, R. *Adv. Mater.* **1990**, *2*, 141.
(14) Kranig, W.; Boeffel, C.; Spiess, H. W. *Liq. Cryst.* **1990**, *8*, 375.
(15) Kranig, W. Ph.D. Thesis, Universität Mainz, 1990.
(16) Voigt-Martin, I. G.; Durst, H. *Liq. Cryst.* **1987**, *2*, 601.
(17) Fischer, E. W.; Orth, H. *Makromol. Chem.* **1965**, *88*, 1881.
(18) Voigt-Martin, I. G.; Andrews, E. H. *Proc. R. Soc.* **1972**, *A327*, 251.
(19) Crewe, A. V.; Isaacson, M. S.; Zeitler, E. In *Advances in Structure Research*; Hoppe, W., Mason, R., Eds.; Pergamon: New York, 1976, Vol. 7.
(20) Cowley, J. M. *Diffraction Physics*; North-Holland: Amsterdam, The Netherlands, 1984.
(21) Hoppe, W.; Hegerl, R. *Topics in Current Physics*; Springer-Verlag: Berlin, FRG, 1980.
(22) Van Dyck, D. *J. Microsc.* **1980**, *119*, 141.
(23) Brillouin, L. *Wave Propagation in Periodic Structures*; Dover: New York, 1946.
(24) Cowley, J. M.; Moodie, A. F. *Acta Crystallogr.* **1967**, *10*, 609.
(25) Cowley, J. M.; Moodie, A. F. *Proc. R. Soc. London* **1958**, *71*, 533.
(26) Voigt-Martin, I. G.; Krug, H.; Van Dyck, D. *J. Phys. Fr.* **1990**, *51*, 2347.
(27) Voigt-Martin, I. G.; Durst, H. *Macromolecules* **1989**, *22*, 168.
(28) Voigt-Martin, I. G.; Durst, H.; Krug, H. *Macromolecules* **1989**, *22*, 595.
(29) Gonzalez, R.; Wintz, P. *Digital Image Processing*; Addison-Wesley: Reading, MA, 1987.
(30) Misell, D. L. *Image Analysis, Enhancement and Interpretation*; North-Holland: Amsterdam, The Netherlands, 1978.
(31) Jähne, B. *Digitale Bildverarbeitung*; Springer-Verlag: Berlin, FRG, 1989.
(32) Van Dyck, D. *Phys. Status Solidi B* **1975**, *72*, 321.
(33) Van Dyck, D.; Coene, W. *Ultramicroscopy* **1984**, *15*, 29.
(34) Henderson, R.; Baldwin, J. M.; Downing, K. H.; Lapault, J.; Zemlin, F. *Ultramicroscopy* **1968**, *19*, 147.
(35) Peterson, I.; Steitz, R.; Krug, H.; Voigt-Martin, I. G. *J. Phys. Fr.* **1990**, *51*, 1003.
(36) Selinger, J.; Bruinsma, R. *Phys. Rev. A* **1991**, *43*, 2910.
(37) Downing, K.; Grano, A. *Ultramicroscopy* **1982**, *7*, 381.
(38) Voigt-Martin, I. G.; Mijlhoff, F. C. *J. Appl. Phys.* **1976**, *47*, 3942.

Registry No. $HO_2C(CH_2)_{14}CO_2H$/tetrakis(heptyloxy)triphenylene (copolymer), 137464-58-5; heptakis(heptyloxy)triphenylene, 69079-53-4.